

Cite this: *Green Chem.*, 2014, **16**, 1507

Hydrothermal catalytic processing of saturated and unsaturated fatty acids to hydrocarbons with glycerol for *in situ* hydrogen production

Derek R. Vardon,^{*a} Brajendra K. Sharma,^b Humberto Jaramillo,^a Dongwook Kim,^c Jong Kwon Choe,^a Peter N. Ciesielski^d and Timothy J. Strathmann^a

Lipids are a promising feedstock to produce renewable hydrocarbon fuels and H₂ via catalytic hydrothermal processing. Upon exposure to hydrothermal media (e.g., 300 °C, 8–11 MPa), lipids rapidly hydrolyze to produce saturated and unsaturated free fatty acids in varying ratios, depending on the feedstock, as well as glycerol. This report demonstrates the potential of Pt–Re/C for the hydrothermal conversion of saturated and unsaturated fatty acids to hydrocarbons, using glycerol reforming for *in situ* H₂ production to meet process demands. Experiments showed that deoxygenation of stearic acid, a model saturated fatty acid, was significantly enhanced with Pt–Re/C under a reducing atmosphere compared to Pt/C. The coupled hydrogenation and deoxygenation (HYD–DOX) of oleic acid, a model unsaturated fatty acid, was also moderately enhanced under an inert atmosphere using glycerol for *in situ* H₂ production, with DOX as the rate-limiting step. Characterization of Pt–Re/C showed that Re had a significant effect on CO : H uptake ratio (2.2) compared to commercial Pt/C (1.3), with the metals dispersed as small crystallites (~3–4 nm) throughout carbon support. Experiments revealed that the initial system H₂ headspace loading <3.45 MPa greatly enhances fatty acid DOX kinetics via decarboxylation/decarbonylation without net H₂ consumption. At higher initial H₂ loadings (\geq 3.45 MPa), fatty acid reduction was also observed as a minor DOX pathway. Experiments also showed that oleic acid HYD–DOX and glycerol reforming are affected by initial glycerol concentration and catalyst loading. Under optimized process conditions, complete HYD–DOX of oleic acid to heptadecane was achieved within 2 h with a net-zero H₂ consumption using a 1 : 3 glycerol-to-fatty acid ratio (*i.e.*, the native ratio in triacylglycerides). X-ray photoelectron spectroscopy showed that H₂ in the reactor headspace results in lower oxidation states of Pt and Re, suggesting a possible mechanism for enhanced DOX kinetics. This approach holds promise for overcoming the high external H₂ demands of conventional lipid hydrotreatment processes.

Received 31st August 2013,
Accepted 19th December 2013

DOI: 10.1039/c3gc41798k
www.rsc.org/greenchem

1. Introduction

With the effect of global climate change increasingly evident, there is a pressing need to transition to renewable fuels and petrochemical substitutes. Green diesel (*e.g.*, renewable diesel-grade hydrocarbons) produced from lipid feedstocks is a potential alternative for partially displacing the 46 billion gallons per year of petroleum diesel consumed in the United States.¹ Green diesel has several advantages over conventional

fatty acid methyl esters (*i.e.*, biodiesel), including their direct compatibility with existing refinery operations, full integration into the transportation infrastructure, and improved fuel performance properties.² Commercialization of green diesel by catalytic hydrodeoxygenation (HDO) has been pursued by Neste Oil's NExBTL and UOP/Eni's Ecofining processes. However, the high moisture content of many lipid-rich feedstocks (*e.g.*, microalgae, waste grease) can be problematic for downstream processing operations, requiring energetic and costly pretreatment and separation steps. In addition, the HDO process has high H₂ process demands because oxygenated lipid functional groups are primarily removed by catalytic reduction.^{3,4} For example, the Ecofining process requires 1.5–3.8 wt% H₂ of the incoming feed stream for vegetable oil upgrading.² The large H₂ demand necessitates colocation with hydrogen production facilities and negatively impacts the process sustainability since H₂ is primarily derived from fossil fuels.^{3,4} As a result, alternative lipid processing routes are being explored for green diesel production.

^aDepartment of Civil and Environmental Engineering, University of Illinois at Urbana-Champaign, 205 N. Mathews Ave., Urbana, IL 61801, USA.

E-mail: dvardon2@illinois.edu; Tel: +1(217) 766-3916

^bIllinois Sustainable Technology Center, University of Illinois at Urbana-Champaign, 1 Hazelwood Dr., Champaign, IL 61820, USA

^cDepartment of Chemistry, Korea Military Academy, Seoul 139-799, Republic of Korea

^dNational Renewable Energy Laboratory, 15013 Denver West Parkway, Golden, CO 80401, USA

Catalytic hydrothermal processing is a promising method for producing renewable hydrocarbons from lipids by utilizing water as the reaction medium.^{5–8} Under subcritical conditions (200–374 °C, 5–20 MPa), water becomes a unique reaction medium with a reduced dielectric constant, providing lipid solubility similar to non-polar solvents.⁹ The interphase mass transfer and water self-dissociation constant increase, creating a highly reactive processing environment.⁹ Additionally, water as a solvent is well suited for high-moisture waste lipid feedstocks such as fish and animal fat processing residues,¹⁰ sewage sludge,¹¹ and algal biomass.¹² Algae are a particularly promising feedstock due to their high lipid productivity rates compared to terrestrial biomass, potential integration with wastewater treatment, and ability to use non-arable land for cultivation.^{12–14}

Triacylglycerides (TAGs), the predominant component of neutral lipids, rapidly hydrolyze in hydrothermal media to produce saturated and unsaturated free fatty acids (FFAs) (e.g., lauric, palmitic, palmitoleic, stearic, oleic, linoleic) in varying ratios, depending on the feedstock, as well as glycerol. Recent work has shown that saturated fatty acids (e.g., lauric, palmitic, stearic) rapidly undergo catalytic deoxygenation (DOX) to produce linear hydrocarbons and CO₂ via decarboxylation/decarbonylation without external H₂ addition over Pt/C and Pd/C catalysts, with Pt/C displaying significantly greater DOX activity.^{5,6} In contrast, oleic acid (mono-unsaturated C18 fatty acid) does not readily undergo DOX under the same conditions. Instead, only partial hydrogenation (HYD) is observed, with stearic acid (saturated C18 fatty acid) being the primary reaction product.^{5,6} Complete conversion of unsaturated fatty acids to renewable hydrocarbons is not achieved, suggesting that olefin HYD (a H₂-consuming reaction) is necessary prior to DOX with noble metals on activated carbon.

In addition, other studies have examined hydrothermal catalytic reforming of glycerol, a by-product of TAG hydrolysis, to generate H₂, commonly referred to as aqueous phase reforming (APR).^{15–20} Typically, glycerol is assumed to be derived as a by-product from biodiesel production. However, utilization of glycerol APR for *in situ* H₂ production may facilitate unsaturated fatty acid HYD, allowing for subsequent fatty acid DOX (HYD–DOX). Furthermore, the addition of Re to Pt/C has been shown to enhance glycerol APR by reducing the affinity for CO,^{18,21} which may allow for improved turnover frequency. Increased CO turnover frequency may enhance fatty acid DOX via decarbonylation, since CO is a reaction by-product;^{22,23} however, to our knowledge the use of Pt–Re/C for

the conversion of saturated and unsaturated fatty acids to hydrocarbons with integrated glycerol APR for *in situ* H₂ production has not been investigated.

This study examines the use of Pt–Re/C for the hydrothermal deoxygenation of stearic acid, a model saturated fatty acid, as well as the coupled hydrogenation and deoxygenation (HYD–DOX) of oleic acid, a model unsaturated fatty acid, with *in situ* H₂ production from glycerol. Experiments were conducted to (i) evaluate the material properties of Pt–Re/C and its stability in hydrothermal media, (ii) determine the use of Re as a promoter metal to enhance saturated fatty acid DOX and generate H₂ *in situ* from glycerol to facilitate complete HYD–DOX of unsaturated fatty acids, (iii) investigate the influence of initial H₂ gas addition on fatty acid HYD–DOX kinetics, reaction pathways, catalyst oxidation state, and net H₂ consumption, and (iv) explore the impact of glycerol and catalyst loading on product yields. Results support a proposed reaction scheme for one-pot hydrothermal catalytic conversion of TAGs to liquid hydrocarbon fuels, involving hydrolysis and catalytic reforming, hydrogenation, and deoxygenation reactions.

2. Results and discussion

2.1. Catalyst characterization

Commercial Pt/C and as prepared Pt–Re/C catalysts were initially characterized to determine their material properties. The metal loading of commercial Pt/C as received was 5 wt% nominal. Pt–Re/C was prepared by aqueous deposition of Re onto commercial Pt/C, followed by *in situ* reduction. This method produced a catalyst with a Pt loading of 5.2 wt% and a Re loading of 4.2 wt% (Pt–Re molar ratio of 1.2), as measured by ICP.

Multipoint N₂-physisorption provided additional information regarding the catalyst support properties, as shown in Table 1. BET analysis determined that commercial Pt/C had a support surface area of 1075 m² g⁻¹, while BJH desorption analysis determined that the pore volume was 0.715 cm³ g⁻¹, with an average pore diameter of 10.23 Å. The addition of Re to commercial Pt/C reduced the support surface area to 750 m² g⁻¹ and the pore volume to 0.607 cm³ g⁻¹, while the average pore diameter remained fairly constant 10.06 Å. The reduction in surface area and pore volume is not atypical for high secondary metal loadings, which may result in pore blockage.²⁴

Recent work by our group to prepare Ru–Sn/C from commercial Ru/C by incipient wetness with SnCl₂ also resulted in a

Table 1 Physisorption and chemisorption parameters for commercial Pt/C, Pt–Re/C as prepared, and Pt–Re/C following hydrothermal exposure

Catalyst	S _{BET} (m ² g ⁻¹)	Pore volume ^a (cm ³ g ⁻¹)	Avg. pore dia. ^a (Å)	CO uptake (μ mol g ⁻¹)	H uptake (μ mol g ⁻¹)	CO : H uptake ratio	Dispersion ^c (%)
Pt/C commercial	1075	0.715	10.23	130	102	1.3	51
Pt–Re/C as prepared	750	0.607	10.06	112	52	2.2	42
Pt–Re/C HT exposure ^b	675	0.507	10.04	84	30	2.8	32

^a Pore volume and average pore diameter determined by BJH desorption. ^b Hydrothermal exposure at 300 °C for 3 h. ^c Dispersion calculated based on CO chemisorption.

decrease in surface area by $268 \text{ m}^2 \text{ g}^{-1}$, without *in situ* reduction; however, for Pt-Re/C, the influence of hydrothermal *in situ* reduction may also be a factor.

CO and H₂ pulse chemisorption was then performed to evaluate catalyst metal site properties, as shown in Table 1. The measured value of irreversible CO uptake for commercial Pt/C was $130 \mu\text{mol g}^{-1}$, slightly greater than the value for H uptake ($112 \mu\text{mol g}^{-1}$). This resulted in a calculated metal dispersion of 51% for Pt/C, based on CO uptake and an assumed CO : M ratio of unity. The addition of Re moderately lowered the measured CO uptake by 13% ($112 \mu\text{mol g}^{-1}$), with a calculated metal dispersion of 42% based on Pt loading. This suggests an increase in particle size, similar to findings from XRD and SEM-EDS described below, or Re coverage of Pt sites during secondary metal loading. In contrast to CO uptake, the

H uptake with Pt-Re/C was markedly reduced by 49% ($52 \mu\text{mol g}^{-1}$) compared to commercial Pt/C. The reduction of H uptake by nearly two-fold (CO : H uptake ratio of 2.2) is similar to previous findings by Simonetti *et al.* (CO : H uptake ratio of 2.3),²⁵ which confirms the significant influence of Re addition and suggests Pt-Re alloy formation.²⁶

XRD analysis of unloaded activated carbon, commercial Pt/C, and Pt-Re/C as prepared provided additional information regarding long-range order and average metal crystallite size, as shown in Fig. 1. Distinct peaks were observed on the bare carbon support, while the lack of sharp, pronounced peaks with Pt/C and Pt-Re/C suggests that the metals were highly dispersed as small crystallites. In comparison to Pt/C, Pt-Re/C displayed a broad XRD peak near 40° (2θ value), with a bulk metal crystallite size of $\sim 3.4 \text{ nm}$ estimated by the Scherer equation.

Pt-Re/C was further characterized to evaluate the nature of bimetallic crystallites after aqueous adsorption and *in situ* reduction. Scanning electron microscopy coupled to energy dispersive X-ray spectroscopy (SEM-EDS) provided a general survey of the Pt and Re distribution across several carbon support particles, as shown in Fig. 2a–d. Although small crystallites comprised predominantly of rhenium were evident, overall both metals were fairly well dispersed throughout the support.

Transmission electron microscopy (TEM) of Pt-Re/C revealed disperse metal crystallites $< 5 \text{ nm}$ in diameter (Fig. 3a), consistent with crystallite size estimates from XRD. The distribution of Pt and Re within individual metal crystallites was also evaluated using scanning transmission electron microscopy coupled to energy dispersive X-ray spectroscopy (STEM-EDS), as shown in Fig. 3b and 3c. EDS analysis confirmed that Pt and Re were present throughout the crystallites, but a fixed metallic ratio was not observed. Based on these results, it was evident that Pt and Re were well dispersed and largely co-localized throughout the support; however, a definitive assessment of the atomic scale, bimetallic crystallite

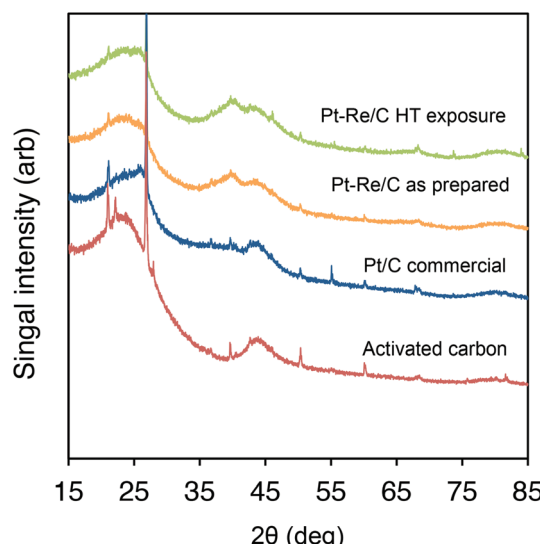


Fig. 1 XRD spectra of unloaded activated carbon, commercial Pt/C as received, Pt-Re/C as prepared, and Pt-Re/C after exposure to hydrothermal media.

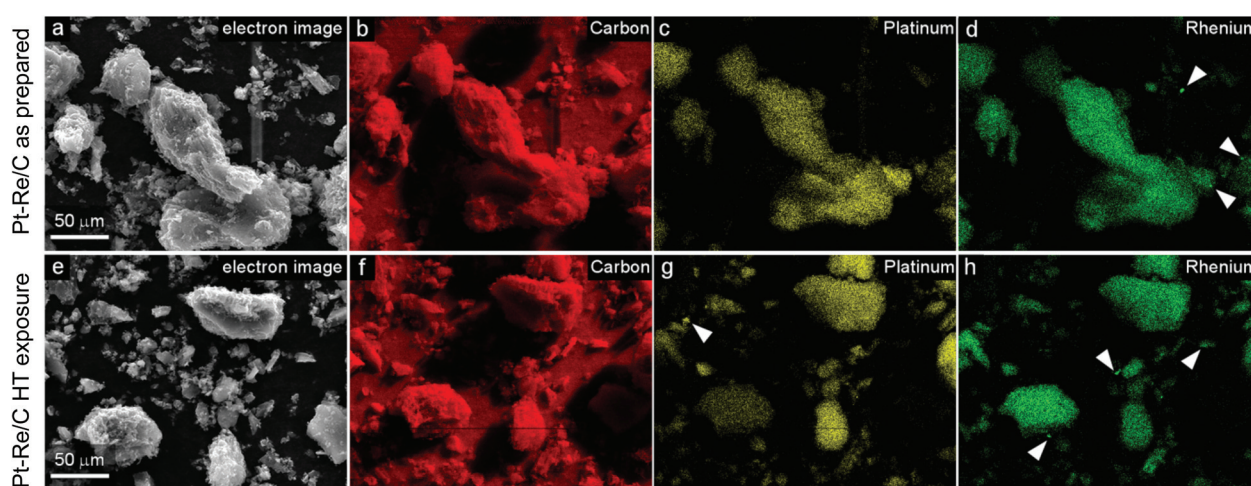


Fig. 2 SEM images and EDS maps of Pt-Re/C catalyst particles as prepared (a–d) and post hydrothermal media exposure (e–h), with single-metal crystallites indicated by white arrowheads.

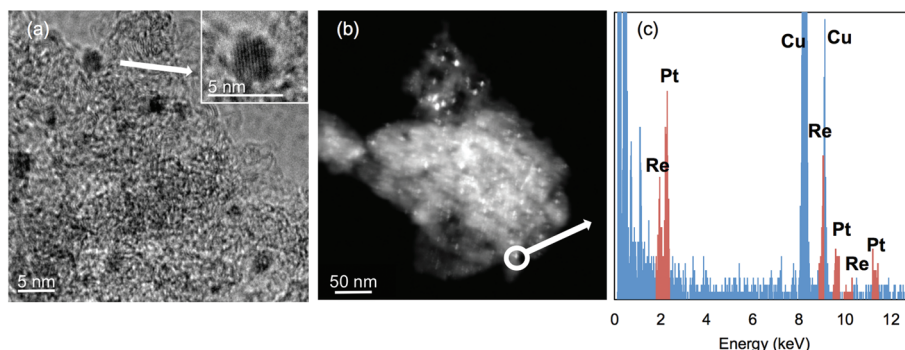
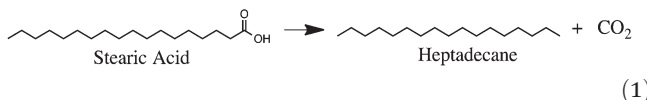


Fig. 3 Pt–Re/C images of the catalyst as prepared by TEM (a) and STEM (b), with localized STEM-EDS spectra obtained from the region of an individual crystallite (c). Note that Cu peaks present due to STEM sample holder.

composition (*e.g.*, collocated mono-metallics, intermetallic alloys, core-shell bimetallics, *etc.*) could not be concluded from this data.

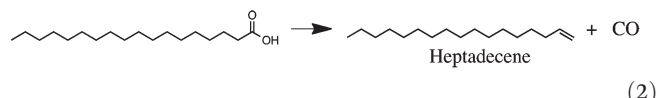
2.2. Catalyst activity

2.2.1. Stearic acid DOX with Pt/C and Pt-Re/C. The influence of Re on the activity of Pt/C for stearic acid DOX was initially investigated, as shown in Rxn. 1, since saturated fatty acids can comprise a significant component of lipids.

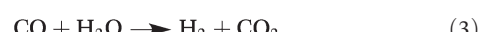


Experiments were performed with Pt/C and Pt-Re/C using a reducing H₂ headspace (<3.45 MPa/557 mmol H₂), as shown in Fig. 4. The conversion of stearic acid to heptadecane at 300 °C occurred with high selectively (>90% molar yield) to heptadecane for both Pt and Pt-Re/C, with octadecane observed in trace amounts (3–8% molar yield). The high selectivity to heptadecane suggests decarboxylation/decarbonylation as the primary DOX pathway,^{3,4} similar to past findings by Fu *et al.* using Pt/C with an inert N₂ headspace.⁵ The main

reaction products from fatty acid decarbonylation (Rxn. 2),^{22,23} terminal alkenes and CO, were not detected in significant amounts.



However, CO can be rapidly converted to CO₂ by the WGS reaction, and terminal alkenes can be readily hydrogenated with a H₂ headspace, as shown in Rxn. 3 and Rxn. 4, respectively.



In contrast to hydrothermal media, organic solvents (*e.g.*, dodecane) produce CO as the primary C-gas product during fatty acid DOX with a H₂ headspace, since the DOX pathway sharply shifts from decarboxylation to decarbonylation.^{22,23} This may be problematic due to competitive adsorption of CO

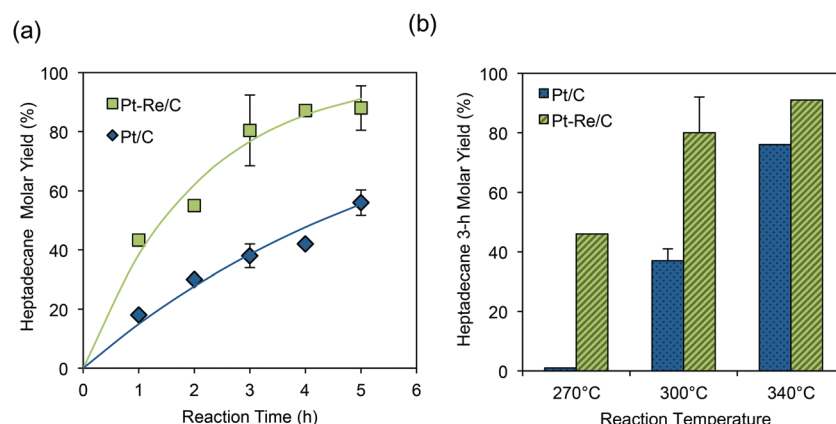


Fig. 4 Timecourse for stearic acid DOX at 300 °C with an initial H₂ reactor headspace using Pt/C and Pt-Re/C (a). Pseudo-first order kinetic parameter fits for heptadecane formation indicated by color solid lines for Pt-Re/C (green) and Pt/C (blue). Effect of temperature on stearic acid DOX 3 h heptadecane molar yields using Pt/C and Pt-Re/C with an initial H₂ reactor headspace (b). Reaction conditions: 20 g stearic acid, 0.5 g catalyst, 80 g H₂O, initial head-gas = 3.45 MPa H₂.

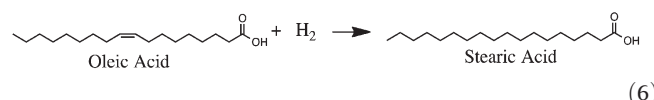
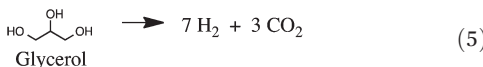
on active catalyst sites and the lack of H₂ regeneration by the WGS reaction in organic media.²⁷

The addition of Re to Pt/C had a significant effect on the apparent stearic acid DOX kinetics at 300 °C, as shown in Fig. 4a. The Pt-Re/C stearic acid pseudo-first order DOX rate constant for the given liquid reactant loading, normalized to catalyst loading ($k_{app\ Pt-Re/C\ DOX} = 2.72 \pm 0.24 \times 10^{-4}\ s^{-1}\ g^{-1}$), was nearly 3-fold greater compared to Pt/C ($k_{app\ Pt/C\ DOX} = 0.94 \pm 0.05 \times 10^{-4}\ s^{-1}\ g^{-1}$). Although multi-phase reaction kinetics are significantly more complex than a pseudo-first order assumption, this simplification allowed for generalized activity comparisons. In addition, Pt-Re/C also displayed improved DOX performance at low temperatures (*i.e.*, <340 °C), as indicated by the heptadecane 3 h molar yields shown in Fig. 4b.

Due to the limitations of collecting accurate hydrothermal kinetic data in a large batch reactor, detailed kinetic analysis was not addressed. Multiple factors can potentially mask intrinsic catalytic activity in batch, including partial deactivation with time on stream, inhibition from reaction by-products, and artifacts introduced during the time delay for batch reactor heat-up.²⁸ However, the effect of Re addition on catalyst activity was pronounced and in-depth kinetic analysis will be addressed in follow-up work.

The increased activity with Re addition may be due to a number of factors, including enhanced CO turnover for decarbonylation as a DOX pathway, alteration to active site morphology, or changes to active site electronic properties. Previous work has shown that addition of Re to Pt/C can significantly reduce CO adsorption affinity,^{18,21} which may allow for greater active site turnover and availability for fatty acid DOX and glycerol reforming reactions. As a control, the activity of the Re precursor alone was tested for stearic acid DOX, with no conversion to heptadecane observed. This suggests that Re may only function as promoter metal with Pt, although further investigation into the mechanism for stearic acid DOX in hydrothermal media is needed.

2.2.2. Glycerol for facilitating oleic acid HYD-DOX. The utilization of glycerol APR for *in situ* H₂ production (Rxn. 5) was then examined to facilitate HYD of oleic acid to stearic acid (Rxn. 6), and subsequent fatty acid DOX (Rxn. 1). Ideally, *in situ* H₂ production from glycerol would alleviate the need for external H₂ consumption, which is problematic for conventional lipid hydrotreatment processes.^{3,4}



Pt/C and Pt-Re/C catalysts were tested with a reactor headspace initially pressurized with N₂ gas (0.35 MPa/56 mmol) at a reaction temperature of 300 °C, as shown in Table 2. With Pt/C and no glycerol addition, oleic acid was only partially hydrogenated (31% molar yield) to stearic acid, similar to findings by Fu *et al.*⁵ Based on the oleic acid loading (71 mmol), 22 mmol of H₂ was required to account for hydrogenation of the single olefin bond in oleic acid. It has been suggested that water, the carbon support, or organic reactants may serve as potential H₂ sources in hydrothermal media.^{5,6,29} Hydrocarbon products resulting from fatty acid DOX were not observed (*e.g.*, heptadecane, octadecane, or lower hydrocarbons). Likewise, analysis of the reactor headspace gas following the reaction revealed no significant quantities (<1 mmol) of H₂ remaining. Therefore, it is presumed that the small amount of H₂ generated *in situ* was consumed by HYD of oleic acid.

In contrast, when glycerol (5 g/54 mmol) was added to the reactor with Pt/C, complete HYD of oleic acid was observed and partial DOX of the resulting stearic acid occurred (24% molar yield), producing heptadecane with high selectivity (>98%). However, heptadecane yields were significantly lower compared to initial experiments with stearic acid in a reducing headspace (Fig. 4), suggesting that the system H₂ level greatly affects catalyst DOX performance. Residual H₂ was also detected in the headspace following the conversion (48 mmol), indicating significant *in situ* H₂ production with glycerol addition. It is estimated that 119 mmol of H₂ was produced *in situ* if the stoichiometric H₂ requirement for oleic acid HYD is added to the measured headspace residual.

Similar to findings with a reducing headspace, the use of Pt-Re/C enhanced stearic acid DOX (38% heptadecane molar yield), although the extent of oleic acid HYD was lower (92% molar yield). As with Pt/C, no significant levels of glycerol remained in the aqueous phase after 9 h for Pt-Re/C. The residual H₂ measured in the headspace (50 mmol) and estimated total *in situ* production (115 mmol; 30% of theoretical

Table 2 Glycerol addition to produce *in situ* H₂ production and promote oleic acid HYD-DOX using Pt/C and Pt-Re/C with an initial inert gas reactor headspace^a

Catalyst	Glycerol loading (g)	H ₂ residual in headspace (mmol)	Oleic acid conversion (%)	Fatty acid and hydrocarbon molar yields	
				Stearic acid (%)	Heptadecane (%)
Pt/C	0	ND	31	31	ND
Pt/C	5	48	100	75	24
Pt-Re/C	5	50	92	53	37

^a Reaction conditions: 300 °C, initial head-gas = 0.35 MPa N₂, 20 g oleic acid, 0.5 g catalyst, 80 g water, time at temperature 9 h. (Note: ND = not detected.)

maximum APR yield) were also similar to yields with Pt/C. As a control, glycerol APR with Pt-Re/C was tested without oleic acid, which produced a comparable level of H₂ (142 mmol; 37% of theoretical), indicating no significant inhibition at the time scale investigated. Past work examining Pt-Re/C solely for glycerol APR found enhanced H₂ productivity (88.7% glycerol conversion, 24.5% H₂ selectivity) compared to Pt/C (5.3% conversion, 56.5% H₂ selectivity);¹⁸ however, a significantly lower temperature was investigated (225 °C).

Analysis of the aqueous phase following the conversion revealed that little residual glycerol remained (<1 wt% of initial loading), suggesting complete decomposition at the elevated temperature (300 °C) and extended reaction time (9 h). The estimated *in situ* production of H₂ represented 31% of the theoretical maximum H₂ yield for glycerol APR (7 H₂ per glycerol). Direct comparisons with previous results for glycerol APR are complicated due to differing temperature regimes, reactor configurations (batch *vs.* continuous), active metals, and catalyst supports. For example, initial investigations with Pt/Al₂O₃ for glycerol APR at 255 °C demonstrated 100% C-conversion to the gas phase with 51% selectivity to H₂. The lower H₂ yield from glycerol observed in this study may be due to undesirable C–O bond cleavage pathways that generate H₂ consuming side-products and prevent CO formation.¹⁸ High temperatures have also been shown to decrease H₂ selectivity during glycerol APR, despite increased conversion.¹⁹ Likewise, higher temperatures can impair the water gas shift (WGS) reaction,³⁰ lowering H₂ yields. However, fatty acid DOX kinetics increase with temperature, following Arrhenius parameters,⁵ suggesting a tradeoff between optimum conditions for glycerol APR and fatty acid DOX.

Based on these results, Pt-Re/C was then chosen for further study due to enhanced acid DOX kinetics compared to Pt/C (Fig. 4 and Table 2), together with past reports of enhanced glycerol APR^{18,20} and reduced affinity for binding CO (Table 1).¹⁸ As noted, CO is produced during fatty acid

decarboxylation and APR of glycerol, and is a known inhibitor of noble metal catalyst activity.³¹

2.2.3. Pt-Re/C activity with an inert and reducing headspace. The reactivity of Pt-Re/C for oleic acid HYD–DOX with *in situ* H₂ production from glycerol was further explored using a reactor headspace initially pressurized with either an inert gas (0.35 MPa/56 mmol N₂) or reducing gas (2.59 MPa/417 mmol H₂) (Fig. 5). With an initial headspace of N₂ (Fig. 5a), oleic acid HYD occurred to a significant extent (91%) after 1.5 h at temperature, followed by a slow progression until completion at 12 h. The H₂ level in the headspace remained fairly constant throughout the reaction (44 ± 4 mmol), and no significant quantities of glycerol were detected in the aqueous phase, indicating that decomposition was complete during reactor heatup to the setpoint temperature. The estimated total *in situ* production of H₂ (measured headspace + estimated stoichiometric demand for oleic acid HYD) was 115 mmol, consistent with findings from catalyst screening experiments. As the reaction progressed, DOX molar yields increased significantly from 7% after 3 h to 38% after 9 h, before leveling off at 41% after 12 h with heptadecane as the primary DOX product (>98% selectivity). The addition of glycerol at high levels (5 g) appeared to have an inhibitory effect on the rate of stearic acid DOX, so pseudo-first order rate constants were not determined. The DOX process progressed much slower compared to HYD of oleic acid and APR of glycerol, suggesting that additional work should target increasing catalytic activity for the former.

With the initial headspace gas switched to H₂ (2.586 MPa/417 mmol), a dramatic enhancement was observed in the apparent rate of oleic acid HYD–DOX with glycerol, as shown in Fig. 5b. Analysis of the reaction products after 1 h at temperature revealed complete HYD, as well as a small amount of DOX (13%). As the reaction progressed, the elevated initial H₂ level greatly enhanced fatty acid DOX kinetics, resulting in complete conversion within 7 h and high selectivity for heptadecane (>98%).

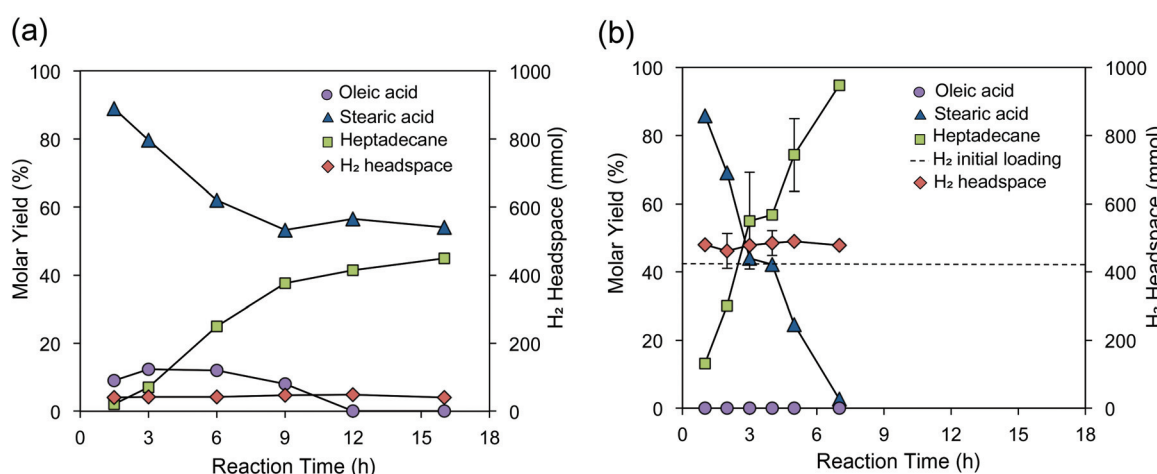
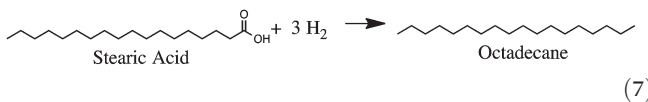


Fig. 5 Hydrothermal catalytic HYD–DOX kinetics of oleic acid using glycerol as an *in situ* H₂ source and an initial reactor headspace containing N₂ (a) and H₂ (b). Reaction conditions: 300 °C, 20 g oleic acid, 5 g glycerol, 0.5 g Pt-Re/C, 80 g H₂O, 0.35 MPa N₂ or 2.59 MPa H₂.

Enhancement of oleic acid HYD–DOX with the addition of H₂ to the headspace was not surprising since oleic acid HYD appears to be a necessary step prior to DOX in hydrothermal media with noble metal catalysts on activated carbon.^{5,6,29} However, it was surprising that headspace analysis revealed a surplus of H₂ (479 ± 9 mmol) in the reactor compared to the initial external loading (417 mmol H₂). After accounting for the extent of oleic acid HYD and final headspace composition, it was estimated that 133 mmol of H₂ was produced *in situ*. Thus, while increased H₂ pressure provides a significant kinetic enhancement, *in situ* H₂ production from glycerol APR exceeded the H₂ consumption requirement for oleic acid HYD and yielded a net positive H₂ balance for the overall catalytic process. It follows that after initial pressurization with H₂, no additional external inputs of H₂ would be required for the catalytic hydrothermal conversion of lipids if H₂ can be recycled in the process.

2.2.4. Influence of initial hydrogen loading. Due to the dramatic influence of H₂ on DOX kinetics, the effect of varying initial H₂ loading (0–5.17 MPa/0–833 mmol) was investigated further by examining the 3 h DOX yields and resulting headspace gas composition. As the initial H₂ reactor loading increased, the 3 h yield of DOX products increased from 7% (0 Pa initial H₂) to 94% (5.17 MPa initial H₂) (Fig. 6a). Heptadecane was observed as the only major DOX product at initial H₂ loadings <3.45 MPa. At higher initial H₂ loadings, fatty acid reduction products (*e.g.*, octadecane, stearic alcohol) were observed (11.3%), indicating a minor shift towards reduction of the carboxylate group as a secondary DOX pathway (Rxn. 7).



The high selectivity for heptadecane observed in hydrothermal media is in contrast to observations reported for organic

solvent media (*e.g.*, dodecane), where selectivity is highly sensitive to H₂ loading. In organic solvents, reaction products are observed from all three fatty acid DOX pathways (*e.g.*, decarboxylation, decarbonylation, reduction) depending on the H₂ loading, with a sharp shift towards decarbonylation as the H₂ partial pressure is increased.^{23,32,33}

Headspace analysis also revealed that the net process H₂ balance was affected by the initial external H₂ loading, as shown in Fig. 6b. At lower initial H₂ loadings (<3.45 MPa/557 mmol), *in situ* H₂ production from glycerol provided a net surplus of system H₂ (net increase of 45 ± 12 mmol) despite the consumption of H₂ by oleic acid HYD (estimated requirement of 71 mmol H₂). However, at high initial loadings of H₂ (≥3.45 MPa/557 mmol), a net reduction in system H₂ was observed after 3 h. The net reduction was attributed to additional H₂ consumption by fatty acid reduction, which consumes 3 moles of H₂ to fully reduce the carboxylate group. In addition, high H₂ pressures can suppress the WGS reaction,³⁴ lowering H₂ production.

Based on these results, the system H₂ pressure, either provided from external sources or produced by *in situ* APR of glycerol, was determined to be a key parameter influencing both fatty acid DOX kinetics and conversion product selectivity. It is also worth noting that the shift in DOX pathways at elevated H₂ pressure suggests that process H₂ levels will be self-limiting, since increasing H₂ pressure will shift conversion towards H₂-consuming reduction processes, preventing further accumulation.

2.2.5. Effect of glycerol and catalyst loading. Additional experiments were then performed to determine the effect of varying glycerol concentrations (Fig. 7a) and catalyst loadings (Fig. 7b) on the 3 h oleic acid HYD–DOX molar yields with *in situ* H₂ production using an initial reducing headspace (2.59 MPa/417 mmol H₂). When no glycerol was added to the reactor, fatty acid HYD was complete and the DOX heptadecane molar yield was still significant (45%) due to the initial

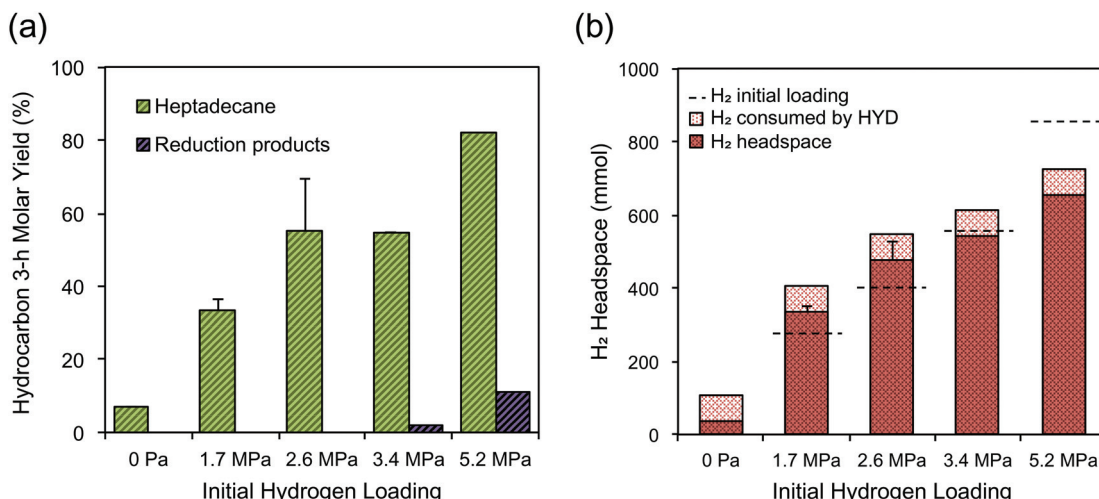


Fig. 6 Influence of initial headspace H₂ loading on oleic acid HYD–DOX (a) and *in situ* H₂ production by glycerol APR (b). Reaction conditions: *t* = 3 h, 300 °C, 20 g oleic acid, 5 g glycerol, 0.5 g Pt–Re/C, 80 g H₂O. H₂ consumed by HYD is estimated based on the observed saturated compounds derived from oleic acid.

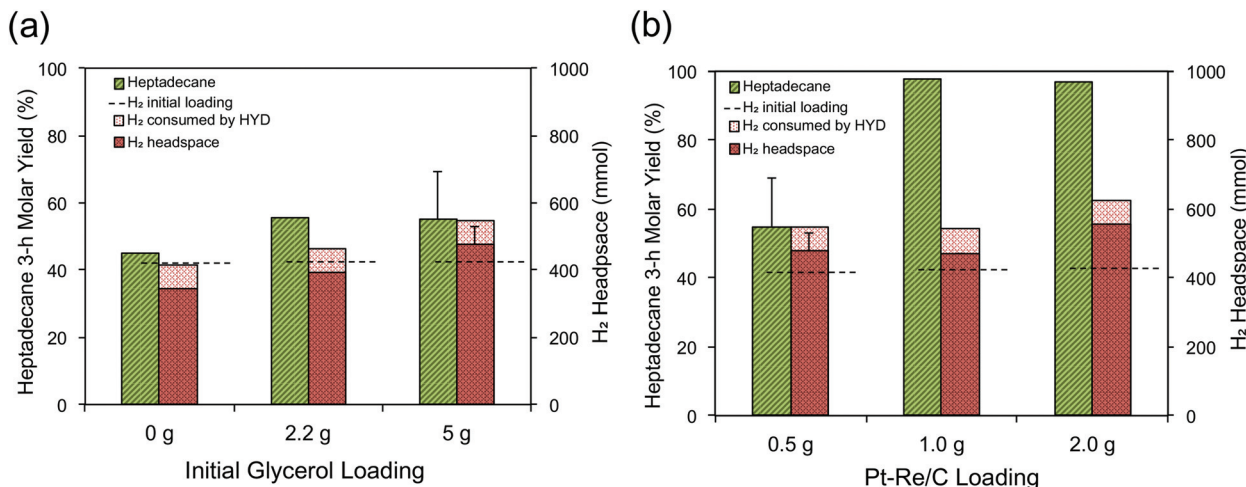


Fig. 7 Influence of glycerol loading (a) and Pt–Re/C loading (b) on 3 h oleic acid HYD–DOX yields and H₂ headspace concentrations. Reaction conditions: 300 °C, 20 g oleic acid, 80 g H₂O, initial H₂ loading = 2.59 MPa, 0.5 g Pt–Re/C loading (for panel a), 5 g glycerol (for panel b).

loading of H₂ in the system; however, the final measured H₂ level (345 mmol) decreased proportionally due to oleic acid HYD. With a glycerol loading (2.2 g) native to the TAG triolein (1 mol of glycerol for every 3 mol of oleic acid), the DOX molar yield increased modestly, resulting in a 3 h molar conversion to heptadecane of 55%. The final headspace H₂ level (394 mmol) dropped below the initial loading (417 mmol); but, to a lesser extent compared to the reaction with no added glycerol (345 mmol). After accounting for H₂ consumption estimated for oleic acid HYD, a total of 48 mmol of H₂ was produced *in situ*. Lastly, a glycerol loading of 5 g (54 mmol) resulted in surplus H₂ in the system (479 ± 9 mmol) compared to the initial loading, with a DOX heptadecane molar yield (55%) comparable to the native triolein loading (2.2 g/24 mmol). The estimated *in situ* H₂ yield was ~30% of the theoretical maximum yield for glycerol APR. After accounting for oleic acid HYD, 133 mmol of H₂ was produced *in situ*. This suggests that further enhancements in glycerol APR activity may be needed to facilitate net zero or net positive system H₂ levels for lipid feedstocks with greater degrees of unsaturation compared to triolein.

Fig. 7b shows the effect of catalyst loading on the 3 h oleic acid HYD–DOX molar yields and *in situ* H₂ production from glycerol. As discussed earlier, the standard catalyst loading used throughout this study (0.5 g) resulted in complete HYD and partial DOX (55%) of oleic acid after 3 h, with a net surplus of H₂ in the headspace (478 mmol \pm 51 mmol). At higher catalyst loadings, the increased number of active sites resulted in a greater degree of fatty acid conversion, as expected. With 1 g of catalyst, complete HYD–DOX of oleic acid to heptadecane occurred with high selectivity (>98%). The yield of *in situ* H₂ remained the same as that observed with 0.5 g catalyst loading, consistent with the observation that glycerol APR has gone to completion for the current sampling time scale. When the catalyst loading was increased to 2 g (1 : 10 fatty acid to catalyst ratio by weight), a modest increase

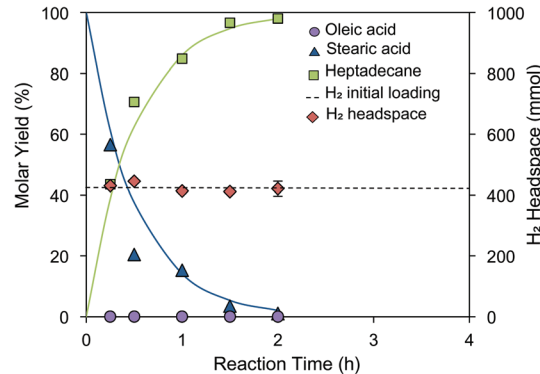


Fig. 8 Timecourse yields for oleic acid HYD–DOX using a glycerol loading native to triolein (1 : 3 glycerol-to-oleic acid molar ratio) and an elevated loading of Pt–Re/C (2.0 g). Other reaction conditions: 300 °C, 20 g oleic acid, 2.2 g glycerol, 80 g H₂O, initial H₂ headspace = 2.59 MPa. Pseudo-first order kinetic parameter fits for stearic acid DOX (blue) to produce heptadecane (green) are shown with solid color lines.

was also observed for *in situ* H₂ production (556 mmol), which resulted in an observed H₂ yield of 47% of the theoretical maximum. This suggests that the glycerol-to-fatty acid ratio for a given catalyst loading may influence *in situ* H₂ yields, although further study is needed.

2.2.6. Native triolein loading. As a demonstration, Fig. 8 shows a final time series experiment conducted for oleic acid using a glycerol loading representative of triolein, a TAG with oleic acid side chains (1 : 3 glycerol-to-oleic acid molar ratio), and an increased catalyst loading (2 g Pt–Re/C) due to enhanced *in situ* H₂ production from glycerol APR (Fig. 7b). Analysis of the reaction products revealed that oleic acid HYD to stearic acid was complete within 15 min at 300 °C (time at which first sample was collected), with a significant extent likely occurring during heat-up from ambient temperature. Despite H₂ consumption from oleic acid HYD, the headspace H₂ level remained fairly constant near the initial loading

(417 mmol), suggesting rapid APR of glycerol and improved H₂ yields compared to earlier results with 0.5 g of catalyst. No significant quantities of glycerol were detected in the aqueous phase after 15 min at temperature. After 2 h at temperature, fatty acid DOX reached completion, significantly faster than the 7 h required with 0.5 g of catalyst despite a higher glycerol loading (5 g glycerol; Fig. 5b). Analysis of the headspace at 2 h confirmed that the overall process was net zero in H₂ consumption (421 ± 25 mmol). The Pt-Re/C stearic acid pseudo-first order DOX rate constant for the given liquid reactant loading, normalized to catalyst loading ($k_{app\ Pt-Re/C\ DOX} = 2.83 \pm 0.38 \times 10^{-4}\ s^{-1}\ g^{-1}$) was comparable to previous results obtained with 0.5 g of catalyst under a reducing headspace without glycerol ($k_{app\ Pt-Re/C\ DOX} = 2.72 \pm 0.24 \times 10^{-4}\ s^{-1}\ g^{-1}$; Fig. 4). The rapid apparent DOX kinetics and lower glycerol loading may mask inhibitory effects of glycerol and its degradation products noted previously. These results demonstrate an initial proof of concept for the catalytic hydrothermal processing of unsaturated TAGs with H₂ consumption requirements being met through APR of glycerol, a byproduct of TAG hydrolysis.

2.3. Influence of headspace composition on Pt-Re oxidation state

The influence headspace gas composition on the Pt-Re oxidation state during exposure to hydrothermal media was then examined due to the pronounced effect on fatty acid DOX kinetics (Fig. 5 and 6). X-ray photoelectron spectroscopy (XPS) was used to characterize the oxidation states of Pt and Re after exposure to hydrothermal media (300 °C, 3 h) with either an inert headspace (0.35 MPa/56 mmol N₂) or a reducing headspace (2.59 MPa/417 mmol H₂). Individual oxidation states of Pt and Re exhibit characteristic doublet pairs due to spin-orbit coupling effects. Metal oxidation states were assessed by comparing binding energy (BE) of the 4f_{7/2} peak against reference standards collected previously,³⁵ as shown in Fig. 9.

Following exposure to hydrothermal media with an inert N₂ headspace, Pt-Re/C was characterized by metals with a high BE and corresponding oxidation state, as shown in Fig. 9a and 9b, respectively. The Pt-Re surface atomic ratio (1.0) determined by XPS was comparable to the bulk ratio measured by ICP (1.2), suggesting a relatively uniform surface and bulk metal ratio throughout the metal crystallites, as opposed to a core-shell orientation. The BE of the 4f_{7/2} peak for Pt was fit with two peaks (71.7 eV, 73.9 eV), indicating a mixed oxidation state based on the range of values previously reported in literature for the NIST XPS database (Pt⁰ = 70.7–71.3 eV; Pt-Re alloy = 71.6–71.8 eV; Pt^{II} = 72.4–74.6 eV).³⁶ The BE of the 4f_{7/2} peak for Re was fit with a single peak (45.6 eV), consistent with a Re^{VII} oxidation state based on Re^{VI} NIST database values (44.3–46.8 eV) and Re^{VII} reference standards previously collected by our group (45.4–46.7 eV),³⁵ despite *in situ* pre-reduction with H₂ at 1.38 MPa for 2 h prior switching the headspace gas over to N₂. This finding agrees with previous work analyzing the oxidation state of Pt-Re/C exposed to

hydrothermal media at lower temperature (225 °C) using *in situ* XPS.²⁰

In contrast to the above, XPS indicated that Pt and Re were in more reduced states following exposure to hydrothermal media with H₂ headspace (2.59 MPa/417 mmol), as shown in Fig. 9c and 9d. The BE of the 4f_{7/2} peak for Pt (71.9 eV) was consistent with a highly reduced state, whereas the measured BE for Re (41.4 eV) was closest to +I reference standard previously collected by our group (41.9 eV).³⁵ Analysis of the Pt-Re surface atomic ratio under a reducing atmosphere (1.0) was identical to the inert headspace above, suggesting no significant changes in crystallite elemental distribution. To our knowledge, this is the first study to examine the effect of H₂ on the oxidation state of Pt-Re/C in hydrothermal media. The lower oxidation states observed with a H₂ headspace may account for the increased activity of the catalyst for DOX processes that are H₂ neutral. However, other factors such as coke minimization, saturation of reaction by-products,³² alteration of carbon support functional groups,^{29,37} or promotion of decarbonylation as a DOX pathway^{22,38,39} may also contribute to the enhanced fatty acid DOX kinetics observed with H₂ reactor headspace.

It is also worth noting that the standard catalyst pre-reduction step used for all reactions in this study (catalyst exposed to 1.38 MPa H₂ for 2 h at 200 °C prior to flushing the headspace and introducing reactants) had a significant effect on the Pt-Re/C fatty acid DOX activity, even when the headspace was initially pressurized with H₂ (2.59 MPa). With catalyst pre-reduction, the 3 h DOX molar yield of heptadecane from oleic acid was 34 ± 3%, compared to 7% without pre-reduction. This contrasts with past studies that reported no enhancement for DOX of saturated fatty acids when Pt/C was pre-reduced (Fu *et al.*, 2010). The difference in DOX performance with Pt-Re/C may be due to rapid re-oxidation of the catalyst after exposure to hydrothermal media with an inert headspace²⁰ or changes in the metal crystallite composition distribution (*i.e.*, alloy formation), as indicated by H₂ chemisorption results.

2.4. Pt-Re/C hydrothermal stability

The stability of Pt-Re/C in hydrothermal media (300 °C, 3 h) with a reducing headspace (2.59 MPa/417 mmol H₂) was then evaluated to determine changes in catalyst composition or morphology. ICP analysis of a representative Pt-Re/C catalyst sample after hydrothermal exposure showed no significant changes in metal loading. Subsequent analysis of the aqueous phase also confirmed that metal leaching was not prominent, although trace levels (<1% of the total metal loading) of Pt and Re initially loaded were observed (Pt = 0.18 ppm; Re = 4.16 ppm).

Analysis of the carbon support by multipoint N₂ physisorption revealed pronounced changes in the surface area, as shown in Table 1. Following hydrothermal exposure, the support surface area of Pt-Re/C decreased by 11% (675 m² g⁻¹), similar to past reports for activated carbon noble metal catalysts in hydrothermal media.^{5,24} Although this decrease is

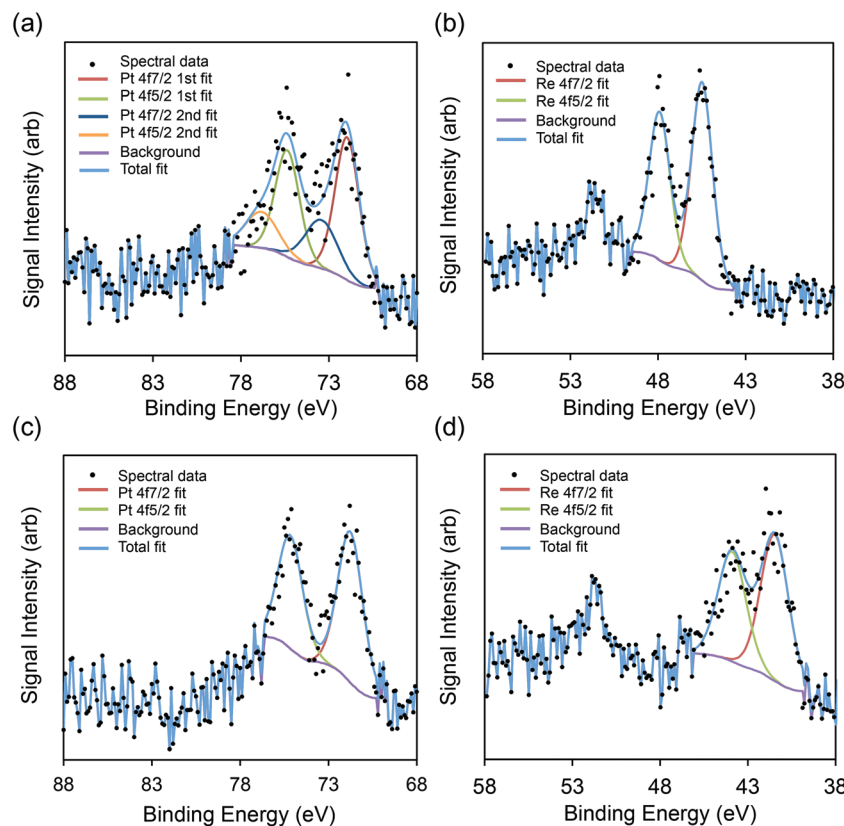


Fig. 9 Influence of an initial inert headspace (0.35 MPa N₂) on the oxidation state of Pt (a) and Re (b), as well as the influence of an initial reducing headspace (2.59 MPa H₂) with Pt (c) and Re (d) after exposure to hydrothermal media for 3 h at 300 °C.

not insignificant, the degree of degradation is much smaller compared to oxide supports which can degrade by over 90% hydrothermal media.⁴⁰ The support pore volume also decreased by 16% (0.507 cm³ g⁻¹), while the average pore diameter remained fairly constant (10.04 Å).

CO and H₂ chemisorption following hydrothermal exposure revealed significant changes to the exposed metal area, as shown in Table 1. Irreversible CO uptake decreased by 25% (CO uptake 84 μmol g⁻¹), resulting in a calculated dispersion of 31.5%. This indicates that high temperature hydrothermal exposure likely results in some sintering of the immobilized metal crystallites, consistent with findings by XRD and SEM-EDS described below. In addition, irreversible H uptake decreased by 42% (H uptake 30 μmol g⁻¹), resulting in a CO : H uptake ratio of 2.8. The high CO : H uptake ratio indicates that Re continues to influence the chemisorption behavior of Pt, although significant morphological changes have occurred compared to as prepared Pt-Re/C.

XRD analysis of Pt-Re/C after hydrothermal media exposure showed support and crystallite peaks similar to the as prepared catalyst (Fig. 1). Estimation of the metal crystallite size by XRD after hydrothermal exposure (3.8 nm compared with 3.4 nm for fresh catalyst) also suggests that sintering occurred. SEM-EDS elemental mapping of Pt and Re revealed that the majority of metallic sites remained co-dispersed, but single-element crystallites were present to a greater degree, as shown

in Fig. 2g and h. These results indicate the need for additional investigation into the hydrothermal stability and activity of Pt-Re/C for fatty acid deoxygenation with time on stream. Although time on stream testing was beyond the scope of this initial study, evaluation of Pt-Re supported on activated carbon pellets for the hydrodeoxygengation of phenol in hydrothermal media demonstrated high stability and activity for over 140 h on stream in a packed bed flow reactor,²⁴ highlighting the potential of Pt-Re/C for facilitating hydrothermal chemistry.

2.5. Integrated reaction scheme

Experimental results support an integrated catalytic hydrothermal reaction scheme for the conversion of lipids to hydrocarbons, with *in situ* H₂ production from glycerol (Fig. 10). As mentioned, in hydrothermal media triacylglycerides rapidly hydrolyze to produce free fatty acids and glycerol. This process is utilized at commercial scale, commonly referred to as fat-splitting.^{41–43} The utilization of hydrolyzed lipids facilitates the use of low-quality lipid feedstocks which are typically high in free fatty acids and problematic for conventional biodiesel processing.⁴⁴ Polar lipids (*e.g.*, phosphatidylcholine) are also known to rapidly hydrolyze to produce free fatty acids, glycerol, and P and N containing moieties,⁴⁵ potentially expanding the range of viable lipid feedstocks for hydrothermal conversion to hydrocarbons.

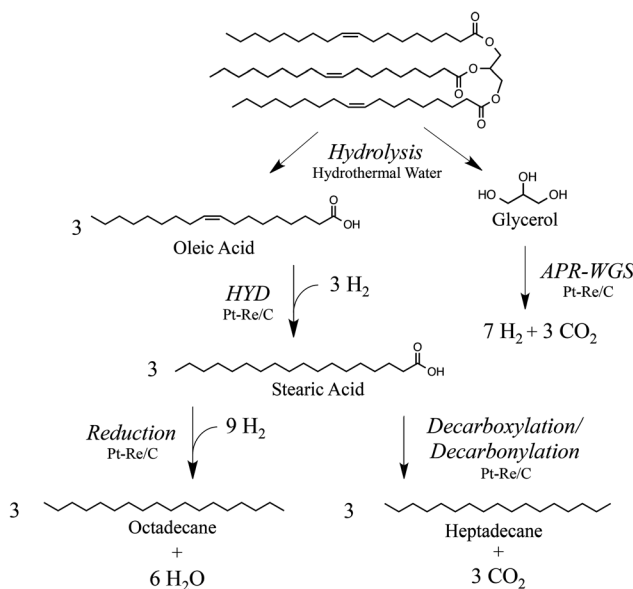


Fig. 10 Proposed reaction scheme and product yields for hydrothermal processing of the triacylglyceride triolein into hydrocarbons and *in situ* H₂.

Following hydrolysis, liberated glycerol can undergo catalytic decomposition reactions to generate H₂ and CO, with CO undergoing the WGS reaction to produce additional H₂ over the appropriate catalyst (Rxn. 5).³⁰ Collectively, aqueous phase reforming can theoretically produce 7 moles of H₂ from 1 mole of glycerol.

As noted, free fatty acids generated from lipid hydrolysis can contain varying ratios of saturated, unsaturated, and polyunsaturated fatty acids, depending on the feedstock origin. For example, waste grease feedstocks (*e.g.*, yellow grease, brown grease, tallow) may contain saturated fatty acids ranging from 39–52% of the total fatty acid profile. Algal lipid feedstocks, in contrast, may contain as low as 10% saturated fatty acids,³ and over 30% polyunsaturated fatty acids depending on the strain.⁴⁶ Fatty acid unsaturation can impart a H₂ consumption demand since HYD to the corresponding saturated fatty acids (Rxn. 6) is necessary prior to DOX of the carboxylic acid group (Rxn. 1 and Rxn. 2). The continuous H₂ demand can potentially be met by APR of glycerol released upon lipid hydrolysis, yielding a net neutral or net positive system H₂ balance. Lipid feedstocks can be blended prior to processing to maintain an optimal degree of unsaturation during continuous processing. Additional H₂ can initially be introduced to accelerate kinetics; however, unlike conventional hydrotreatment processes, continuous H₂ input may not be required.

Saturated fatty acids undergo DOX during catalytic hydrothermal processing to produce linear hydrocarbons with high selectivity. The DOX pathway may progress *via* decarboxylation (Rxn. 1), or decarbonylation (Rxn. 2) rapidly followed by HYD of the terminal alkene (Rxn. 4).

Although terminal alkene HYD includes consumption of H₂, the overall decarbonylation process is H₂ neutral because

the CO produced from the initial decarbonylation yields additional H₂ *via* the WGS reaction (Rxn. 3). In contrast to H₂-neutral decarboxylation and decarbonylation pathways, fatty acid reduction pathways observed at higher initial H₂ loadings (Fig. 3a) consume H₂. Complete fatty acid reduction to the corresponding hydrocarbon consumes 3 moles of H₂ (Rxn. 7).

3. Conclusion

In summary, catalytic hydrothermal processing is a promising method for converting saturated and unsaturated fatty acids into hydrocarbon fuels while using glycerol APR to meet process H₂ consumption needs. To our knowledge, this is the first report demonstrating complete HYD–DOX of unsaturated fatty acids with net zero H₂ consumption using glycerol. Experiments revealed that fatty acid DOX was influenced by the addition of Re to Pt/C, system H₂ level, and glycerol and catalyst loading. Fatty acid decarboxylation/decarbonylation was observed as the primary DOX pathway, with reduction being observed as a minor pathway at high initial H₂ loadings (≥ 3.45 MPa/557 mmol). Although several mechanisms may account for enhanced DOX yields with H₂ initially loaded into the system, the effect on catalyst activity and oxidation state was pronounced. Characterization of Pt–Re/C determined that Re had a significant effect on CO : H uptake ratio (2.2) compared to commercial Pt/C (1.3), with metals dispersed as small crystallites (~3–4 nm) throughout carbon support. Optimized conditions were applied with a 1 : 3 glycerol-to-oleic acid molar ratio (*i.e.*, native ratio formed upon hydrolysis of the TAG triolein), which resulted in complete DOX within 2 h at temperature and net-zero H₂ consumption. Catalyst characterization after hydrothermal exposure revealed that moderate sintering had occurred, suggesting additional work is needed to evaluate Pt–Re/C stability with time on stream. A H₂-neutral (or positive) scheme for hydrothermal catalytic conversion of TAGs is proposed, involving TAG hydrolysis, catalytic reforming of glycerol, and fatty acid hydrogenation and deoxygenation processes resulting in saturated hydrocarbon products. Results from this study suggest a promising strategy for overcoming some of the major limitations of conventional lipid-to-biofuel pathways.

4. Materials and methods

4.1. Materials

Stearic acid (98%) was obtained from TCI Chemicals and oleic acid (90%) was obtained from Alfa Aesar. Glycerol (99.5%), activated carbon (Darco 100 mesh), powdered Pt/C (5 wt%) catalyst, and ammonium perrhenate salt (NH₄ReO₄) were purchased from Sigma-Aldrich. Hydrocarbon standards (*e.g.*, pentadecane, hexadecane, heptadecane, octadecane) were obtained from Chem Service Inc. Analytical-grade dichloromethane (DCM) and methanol were obtained from Fisher Scientific. For a typical experiment, Pt–Re/C was prepared *via*

aqueous adsorption of NH_4ReO_4 onto 0.5 g of Pt/C catalyst suspended in 50 g of deionized (DI) water. The contents were loaded into a Parr 4575 500 mL high temperature/pressure reactor. Pt/C and Pt-Re/C catalysts were pre-reduced *in situ* prior to use by purging and venting the reactor with 1.38 MPa of H_2 over three cycles, followed by heating to 200 °C with continuous mixing for 2 h at temperature. The reactor was then cooled to ambient temperature and maintained under positive pressure with either an inert (N_2) or reducing (H_2) gas.

4.2. Catalyst characterization

Catalyst metal loadings were measured using a Spector Arcos Inductively Coupled Plasma Atomic Emission Spectrometer (ICP-AES) after digestion in concentrated acid. Support surface area, pore volume, and average pore diameter were determined by multipoint N_2 physisorption using a QuandaSorb SI analyzer. Catalyst specific surface area was calculated by BET, and pore volume and pore diameter were calculated by BJH desorption. Prior to analysis, catalysts were outgassed at 250 °C for 18 h. Physisorption measurements were performed at the temperature of liquid N_2 .

Catalyst metal dispersion and the influence of Re on Pt was determined by CO and H_2 chemisorption using a Micromeritics Autochem II 2920 pulse analyzer. Prior to analysis, catalysts were degassed at 40 °C for 0.2 h under Ar, dried at 100 °C, and reduced at 280 °C in flowing 10% H_2/Ar (50 mL min⁻¹) for 1 h. Catalysts were then purged at 280 °C for 0.5 h with either He (for CO chemisorption) or Ar (for H_2 chemisorption). Chemisorption measurements were performed at 45 °C and metal dispersion was calculated based on CO uptake with a CO : M ratio of unity.

Long-range catalyst material order was analyzed by XRD using a Rigaku Ultima IV X-ray diffractometer. The X-ray voltage was set to 40 kV and 44 mA, with a sampling width of 0.02° and scan speed of 5° min⁻¹. Metal crystallite size parameters were estimated using the Scherer equation with PDXL version 1.6.0.1 (Rigaku Corporation).

Imaging and elemental mapping of multiple catalyst particles was performed by SEM-EDS using a FEI Quanta 400 FEG scanning electron microscope equipped with an EDAX X-ray detector. Samples were mounted onto aluminum stubs using a conductive carbon tape to adhere the particles to the stub and provide electrical conductivity. Elemental mapping was performed using an accelerated voltage of 30 kV. The signal was based on net X-ray intensity using a Z absorption fluorescence (ZAF) correction over a dwell time of 300 ms per pixel.

High-resolution TEM images of individual catalyst particles were collected using a JEOL 2010LAB₆ TEM instrument. Samples were dispersed in acetone and mounted onto holey carbon Cu grids prior to analysis. STEM-EDS elemental mapping of metallic crystallites was also performed using a JEOL 2010F field emission TEM instrument, coupled to an Oxford INCA EDS detector with a 1 nm probe size.

Catalyst surface oxidation states were examined using a Physical Electronics PHI 5400 X-ray photoelectron spectrometer equipped with a monochromatized Mg K α source

(1253.6 eV). The pass energy employed for high resolution Pt and Re XPS spectra was 35.8 eV. Pt-Re/C catalysts for XPS analysis were exposed to hydrothermal media (300 °C, 3 h) using the Parr 4575 reactor loaded initially with either an inert (0.35 MPa/56 mmol N_2) or reducing (2.59 MPa/417 mmol H_2) headspace. After exposure, catalysts were sampled *in situ* using a Parr 4532-D collection attachment. The isolation valve on the reactor was briefly released to charge the sampling accessory, which was then cooled to ambient pressure using a water-cooling sleeve. To prevent air exposure, catalyst samples were dried inside an anoxic glove box and loaded onto conductive copper tape located inside an anoxic XPS-sample holder chamber, as described previously.³⁵ High-resolution (*i.e.*, 0.1 eV resolution) XPS spectra were collected from 38.0 eV to 58.0 eV for Re and 68.0 eV to 88.0 eV for Pt. Spectra were energy-normalized relative to the dominant C 1s peak from the activated carbon support (284.5 eV). Spectra were then normalized and fit with a convoluted Gaussian and Lorentzian function after constraining the separation distance and peak area ratio of contributing doublet peaks with CasaXPS version 2.3 (Casa Software Ltd).

4.3. Catalytic hydrothermal processing

Hydrothermal conversions were conducted in the Parr 4575 reactor. The reactor containing pre-reduced catalyst was loaded with the 20 g of oleic acid, and 5 g of glycerol dissolved in 30 g of DI (80 g DI total including water from catalyst pre-reduction). The reactor vessel was pressurized to 1.38 MPa with the desired headspace gas (N_2 or H_2) and purged for three cycles under constant stirring. The headspace pressure was then increased to the desired initial value corrected to 25 °C. Reactor temperature was raised to 300 °C at a rate of ~10 °C min⁻¹ (heat-up time ~1 h) with constant stirring at high speed (>1000 rpm) applied for the desired reaction time. Once the reaction time elapsed, the reactor was rapidly cooled to ambient temperature by initiating water flow through internal cooling coils. For time series studies, independent batch reactions were performed for each time point. Where indicated, triplicate reactions were performed independently to determine experimental variability, with error bars representing standard deviations.

4.4. Reaction product analysis

The total reactor contents were collected, fractionated, and analyzed gravimetrically to ensure mass balance closure of the aqueous and organic product phases. After confirming mass balance closure, the recovered reactor contents were heated while stirring to produce a bi-phase system for sampling. The top organic layer containing fatty acids and hydrocarbons was sampled, dissolved in DCM (1 wt% sample), and filtered (0.45-μm PTFE) prior to analysis to remove catalyst particles. Dissolved glycerol in the bottom aqueous phase was sampled, dissolved in methanol (1 wt% sample) and filtered (0.45-μm PTFE) prior to analysis. As a control, each complete bilayer was also dissolved in excess solvent and analyzed to ensure representative results from sampling.

Fatty acids, alkanes, alcohols, (e.g., stearyl alcohol), glycerol and glycol derivatives (e.g., ethylene glycol, propylene glycol) were quantified using a HP 5890 Series II FID gas chromatograph outfitted with a Restek Stabilwax-DA column (30 m × 0.25-mm id, 0.25-μm film). Helium (6 mL min⁻¹ column flow) was used as the carrier gas with the injector split flow set to 60 mL min⁻¹. The oven temperature was increased from 40 °C to 250 °C at 10 °C min⁻¹. The injector volume was set to 1 μL and the inlet temperature set at 250 °C. The detector temperature was set to 250 °C, H₂ gas set to 32 mL min⁻¹, and airflow set to 400 mL min⁻¹. Compound retention times and FID-calibration response curves were conducted using fatty acid, glycerol, and alkane standards. Reaction products were also confirmed by GC-MS analysis using a Varian 3800 gas chromatograph with a Varian 2000 mass spectrometer and Restek RTX-5MS column and by ¹H NMR using a Varian Unity 400 MHz spectrometer with conditions described previously.⁴⁷

Reactor headspace gas samples were collected after the reaction using 0.5-L Restek Tedlar sample bags, and analyzed for H₂, CH₄, CO, and CO₂ using a HP 5890 Series II TCD gas chromatograph outfitted with a Carboxen-1010 Supelco column. For the carrier gas, N₂ (1 mL min⁻¹) was used to analyze H₂, while He was used to analyze carbon-based gases (1 mL min⁻¹). A split flow of 10 mL min⁻¹ was used with an inlet temperature of 225 °C. An isothermal oven temperature profile was used to detect H₂ (35 °C) and carbon-based gases (125 °C). The TCD detector was set to 225 °C at high sensitivity with a reference gas flow of 15 mL min⁻¹ and auxiliary gas flow of 7 mL min⁻¹.

Hydrocarbon product molar yields were calculated by dividing the moles of recovered product by the moles of fatty acid initially loaded into the reactor. Hydrocarbon selectivities were calculated by dividing the moles of hydrocarbon product by the moles of converted fatty acid. *In situ* H₂ production yields were determined using the ideal gas law based on the final headspace gas pressure and compositional analysis determined by GC-TCD. Due to the low solubility of H₂ in water at ambient temperature compared to the gas loadings examined in this study, dissolved H₂ was assumed to be negligible. For this work, H₂ selectivity from glycerol APR is defined as the ratio of H₂ produced, divided by the theoretical amount of H₂ produced if the converted glycerol was completely reformed (e.g., decomposition and WGS) to generate H₂ and CO₂. Apparent reaction rate constants for stearic acid deoxygenation were estimated assuming pseudo-first order kinetics using non-linear regression with GraphPad Prism version 6.00 (GraphPad Software).

Acknowledgements

The research described in this paper has been funded in part by the United States Environmental Protection Agency (EPA) under the Science to Achieve Results (STAR) Graduate Fellowship Program. The EPA has not officially endorsed this publication and the views expressed herein may not reflect the

views of the EPA. This material is also based upon work supported by the National Science Foundation Graduate Research Fellowship (DGE-1144245). Any opinion, findings, and conclusions or recommendations expressed in this material are those of the authors and do not necessarily reflect the views of the National Science Foundation. In addition, financial support was provided by the Department of Civil and Environmental Engineering at the University of Illinois and the National Science Foundation Division of Chemical, Bioengineering, Environmental, and Transport Systems (CBET-0746453).

We thank Rick Haasch for assistance with XPS analysis at the Center of Microanalysis of Materials (UIUC), which is supported by the U.S. Department of Energy under grant DEFG02-91-ER45439. Catalyst characterization was also supported in part by the Center for Direct Catalytic Conversion of Biomass to Biofuels (C3Bio), an Energy Frontier Research Center funded by the U.S. DOE, Office of Science, Office of Basic Energy Sciences, Award Number DE-SC0000997. Additionally, we would like to thank Martin Menart at the Colorado School of Mines for assistance with catalyst chemisorption measurements.

References

- U.S. EIA, 2011.
- T. N. Kalnes, K. P. Koers, T. Marker and D. R. Shonnard, *Environ. Prog. Sustainable Energy*, 2009, **28**, 111–120.
- A. Berenblyum, V. Danyushevsky, E. Katsman, T. Podoplelova and V. Flid, *Pet. Chem.*, 2010, **50**, 305–311.
- E. Santillan-Jimenez and M. Crocker, *J. Chem. Technol. Biotechnol.*, 2012, **87**, 1041–1050.
- J. Fu, X. Lu and P. E. Savage, *Energy Environ. Sci.*, 2010, **3**, 311–317.
- J. Fu, X. Lu and P. E. Savage, *ChemSusChem*, 2011, **4**, 481–486.
- P. Biller, R. Riley and A. B. Ross, *Bioresour. Technol.*, 2011, **102**, 4841–4848.
- T. M. Yeh, J. G. Dickinson, A. Franck, S. Linic, L. T. Thompson and P. E. Savage, *J. Chem. Technol. Biotechnol.*, 2013, **88**, 13–24.
- A. A. Peterson, F. Vogel, R. P. Lachance, M. Fröling, M. J. Antal, Jr. and J. W. Tester, *Energy Environ. Sci.*, 2008, **1**, 32–65.
- P. Jayasinghe and K. Hawboldt, *Renewable Sustainable Energy Rev.*, 2012, **16**, 798–821.
- M. N. Siddiquee and S. Rohani, *Renewable Sustainable Energy Rev.*, 2011, **15**, 1067–1072.
- L. Brennan and P. Owende, *Renewable Sustainable Energy Rev.*, 2010, **14**, 557–577.
- J. K. Pittman, A. P. Dean and O. Osundeko, *Bioresour. Technol.*, 2010, **102**, 17–25.
- J. A. Lercher, C. Zhao and T. Brueck, *Green Chem.*, 2013, **15**, 1720–1739.

- 15 R. D. Cortright, R. R. Davda and J. A. Dumesic, *Nature*, 2002, **418**, 964–967.
- 16 J. Shabaker, G. Huber and J. Dumesic, *J. Catal.*, 2004, **222**, 180–191.
- 17 N. Luo, X. Fu, F. Cao, T. Xiao and P. P. Edwards, *Fuel*, 2008, **87**, 3483–3489.
- 18 D. L. King, L. Zhang, G. Xia, A. M. Karim, D. J. Heldebrant, X. Wang, T. Peterson and Y. Wang, *Appl. Catal., B*, 2010, **99**, 206–213.
- 19 D. Ö. Özgür and B. Z. Uysal, *Biomass Bioenergy*, 2011, **35**, 822–826.
- 20 L. Zhang, A. M. Karim, M. H. Engelhard, Z. Wei, D. L. King and Y. Wang, *J. Catal.*, 2012, **287**, 37–43.
- 21 E. L. Kunkes, D. A. Simonetti, J. A. Dumesic, W. D. Pyrz, L. E. Murillo, J. G. Chen and D. J. Buttrey, *J. Catal.*, 2008, **260**, 164–177.
- 22 A. S. Berenblyum, T. A. Podoplelova, R. S. Shamsiev, E. A. Katsman and V. Y. Danyushevsky, *Pet. Chem.*, 2011, **51**, 336–341.
- 23 B. Rozmysłowicz, P. Mäki-Arvela, A. Tokarev, A.-R. Leino, K. Eränen and D. Y. Murzin, *Ind. Eng. Chem. Res.*, 2012, **51**, 8922–8927.
- 24 Y. T. Kim, J. A. Dumesic and G. W. Huber, *J. Catal.*, 2013, **304**, 72–85.
- 25 D. A. Simonetti, E. L. Kunkes and J. A. Dumesic, *J. Catal.*, 2007, **247**, 298–306.
- 26 B. H. Isaacs and E. E. Petersen, *J. Catal.*, 1984, **85**, 1–7.
- 27 B. Rozmysłowicz, P. Mäki-Arvela and D. Murzin, in *Biomass Conversion*, ed. C. Baskar, S. Baskar and R. S. Dhillon, Springer, Berlin Heidelberg, 2012, pp. 199–220.
- 28 M. Behrens and A. K. Datye, *Catalysis for the Conversion of Biomass and Its Derivatives*, Max Planck Research Library for the History and Development of Knowledge, 2013.
- 29 J. Fu, F. Shi, L. T. Thompson, X. Lu and P. E. Savage, *ACS Catal.*, 2011, **1**, 227–231.
- 30 R. R. Davda, J. W. Shabaker, G. W. Huber, R. D. Cortright and J. A. Dumesic, *Appl. Catal., B*, 2005, **56**, 171–186.
- 31 R. R. Soares, D. A. Simonetti and J. A. Dumesic, *Angew. Chem., Int. Ed.*, 2006, **118**, 4086–4089.
- 32 J. G. Immer and H. H. Lamb, *Energy Fuels*, 2010, **24**, 5291–5299.
- 33 J. G. Immer, M. J. Kelly and H. H. Lamb, *Appl. Catal., A*, 2010, **375**, 134–139.
- 34 J. W. Shabaker and J. A. Dumesic, *Ind. Eng. Chem. Res.*, 2004, **43**, 3105–3112.
- 35 J. K. Choe, J. R. Shapley, T. J. Strathmann and C. J. Werth, *Environ. Sci. Technol.*, 2010, **44**, 4716–4721.
- 36 NIST, *X-Ray Photoelectron Spectroscopy Database*, 2012.
- 37 H. P. Boehm, *Carbon*, 1994, **32**, 759–769.
- 38 J. Lu, S. Behtash and A. Heyden, *J. Phys. Chem. C*, 2012, **116**, 14328–14341.
- 39 J. Lu, S. Behtash, M. Faheem and A. Heyden, *J. Catal.*, 2013, **305**, 56–66.
- 40 H. N. Pham, A. E. Anderson, R. L. Johnson, K. Schmidt-Rohr and A. K. Datye, *Angew. Chem., Int. Ed.*, 2012, **51**, 13163–13167.
- 41 L. Lascaray, *Ind. Eng. Chem.*, 1949, **41**, 786–790.
- 42 T. A. Patil, D. N. Butala, T. S. Raghunathan and H. S. Shankar, *Ind. Eng. Chem. Res.*, 1988, **27**, 727–735.
- 43 R. L. Holliday, J. W. King and G. R. List, *Ind. Eng. Chem. Res.*, 1997, **36**, 932–935.
- 44 F. Ma and M. A. Hanna, *Bioresour. Technol.*, 1999, **70**, 1–15.
- 45 S. Changi, A. J. Matzger and P. E. Savage, *Green Chem.*, 2012, **14**, 2856.
- 46 M. J. Griffiths and S. T. L. Harrison, *J. Appl. Physiol.*, 2009, **21**, 493–507.
- 47 D. R. Vardon, B. K. Sharma, J. Scott, G. Yu, Z. Wang, L. Schideman, Y. Zhang and T. J. Strathmann, *Bioresour. Technol.*, 2011, **102**, 8295–8303.